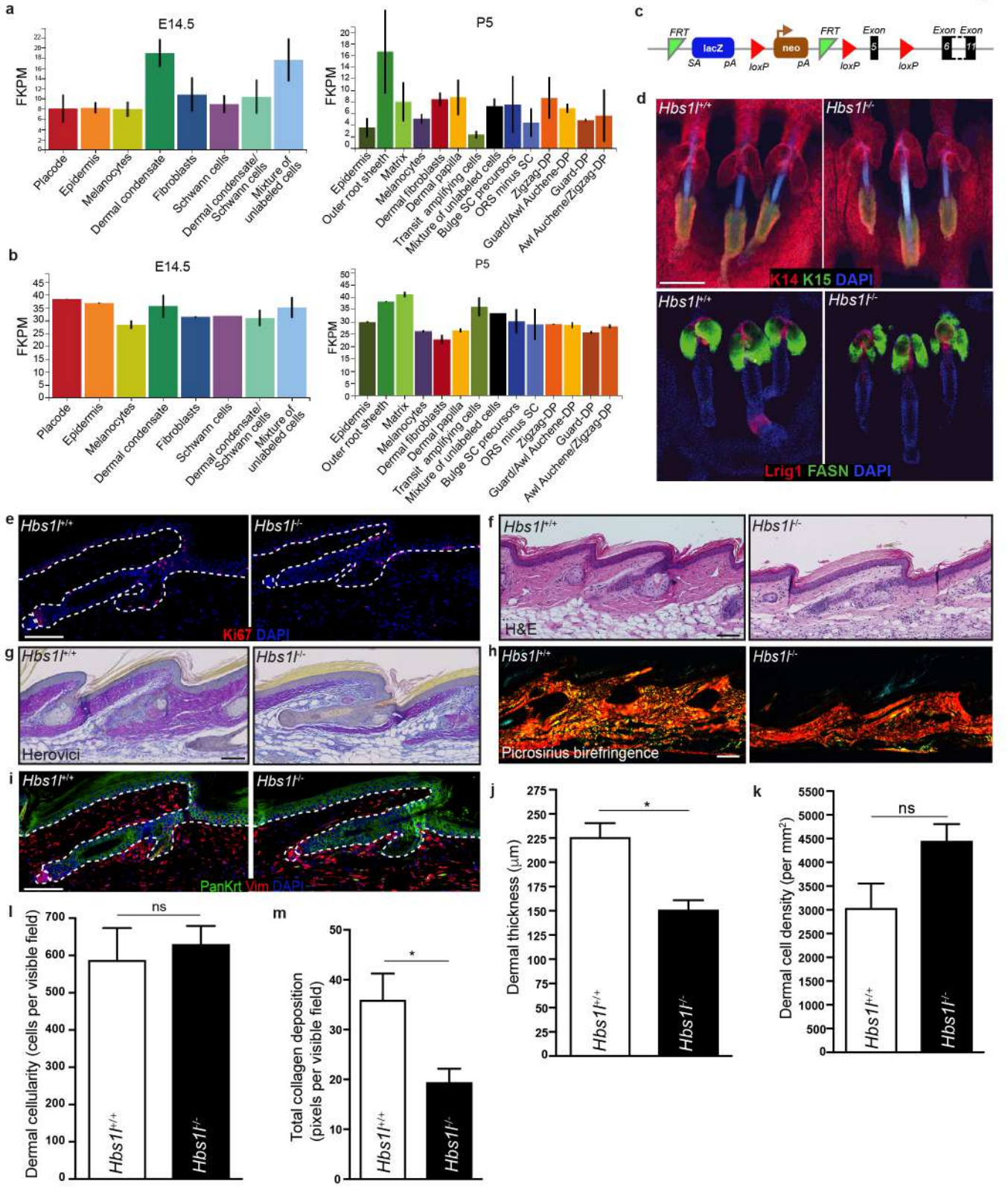
a
E14.5
P5
FKPM
Placode
Epidermis
Melanocytes
Dermal condensate
Fibroblasts
Schwann cells
Dermal condensate/ Schwann cells
Mixture of unlabeled cells
Epidermis
Outer root sheeth
Matrix
Melanocytes
Dermal fibroblasts
Dermal papilla
Transit amplifying cells
Mixture of unlabeled cells
Bulge SC precursors
ORS minus SC
Zigzag-DP
Guard/Awl Auchene-DP
Guard-DP
Awl Auchene/Zigzag-DP
b
E14.5
P5
FKPM
c
FRT
lacZ
SA
pA
loxP
neo
pA
FRT
loxP
Exon
5
loxP
Exon
6
Exon
11
d
Hbs1l+/+
Hbs1l-/-
K14 K15 DAPI
Hbs1l+/+
Hbs1l-/-
Lrig1 FASN DAPI
e
Hbs1l+/+
Hbs1l-/-
Ki67 DAPI
f
Hbs1l+/+
Hbs1l-/-
H&E
g
Hbs1l+/+
Hbs1l-/-
Herovici
h
Hbs1l+/+
Hbs1l-/-
Picrosirius birefringence
i
Hbs1l+/+
Hbs1l-/-
PanKrt Vim DAPI
j
Dermal thickness (μm)
*
Hbs1l+/+
Hbs1l-/-
k
Dermal cell density (per mm2)
ns
Hbs1l+/+
Hbs1l-/-
l
Dermal cellularity (cells per visible field)
ns
Hbs1l+/+
Hbs1l-/-
m
Total collagen deposition (pixels per visible field)
*
Hbs1l+/+
Hbs1l-/-

Extended Data Figure 1. *Pelo* is expressed in all skin cell subpopulations and Knockout of *Hbs1l* leads to mild dermal phenotype (a, b) *Pelo* and *Hbs1l* are ubiquitously expressed in all cell populations of embryonic and neonatal skin. mRNA expression data obtained from hair and skin gene expression library (Hair-GEL; www.hair-gel.net). (c) Schematic of *Hbs1l* knockout-first allele. (d) Immunolabelling of tail epidermal wholemounts with antibodies to Krt14, Krt15, Lrig1 and FASN. (e) Tail skin sections immunolabelled for Ki67, showing no significant change in the distribution of Ki67+ cells in *Hbs1l*$^{-/-}$ epidermis. (f) H&E staining of adult control and *Hbs1l*$^{-/-}$ tail skin. (g) Herovici's polychrome staining to visualize immature (blue) and mature (pink) dermal collagen. (h) Picrosirius staining of tail skin showing the birefringence of collagen fibers against a black background. (i) Immunostaining of tail skin sections with pan-keratin (PanKrt) and vimentin (Vim) antibodies. (j-m) Quantification of dermal thickness (j), dermal cell density (k), dermal cellularity (l) and total collagen deposition (m). Dashed lines mark epidermal-dermal boundary. Scale bars 100 μm. *p = 0.0286 in (j, m). FKPM - Fragments per Kilobase of transcript Per Million mapped reads.

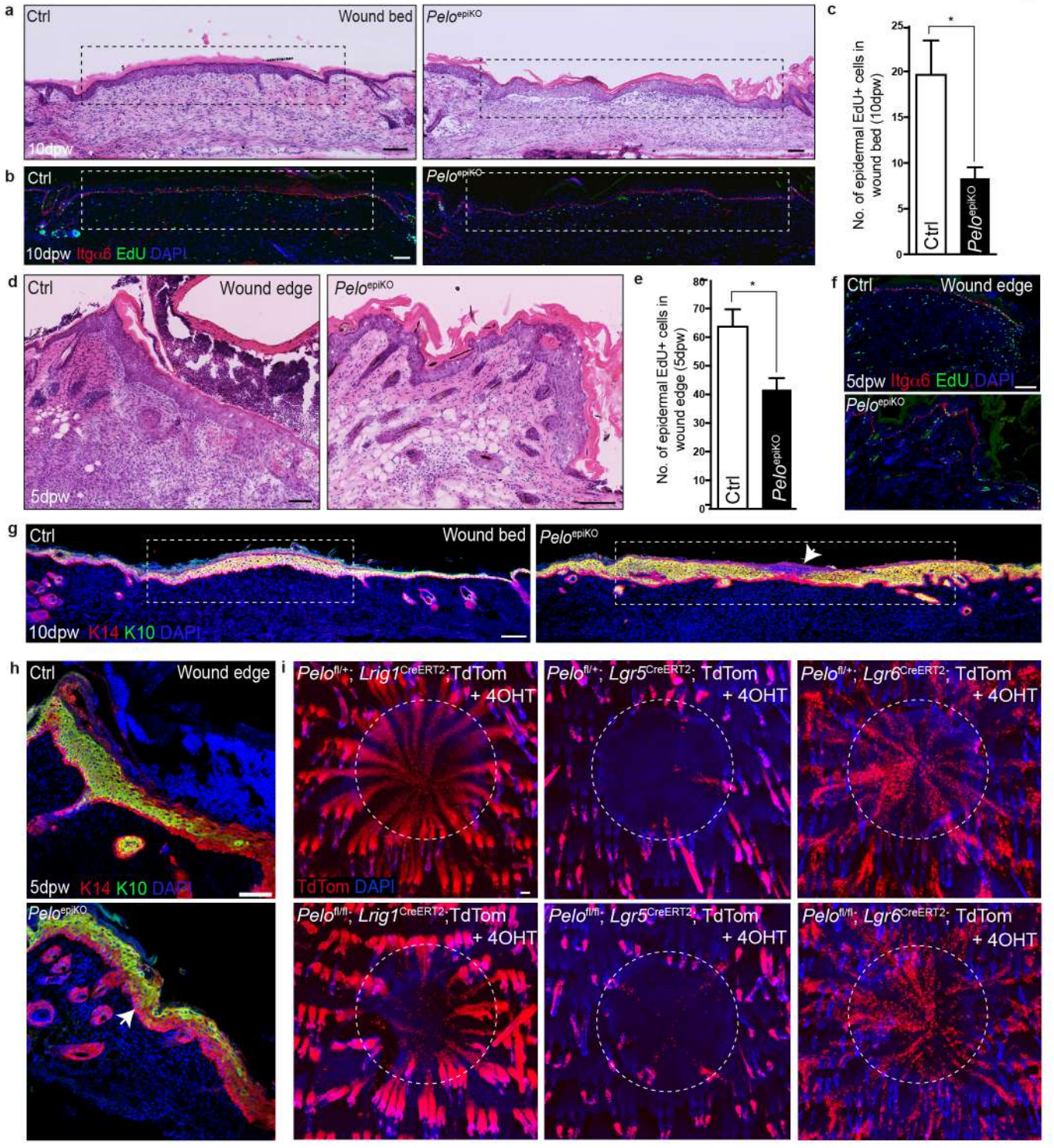
a
Ctrl
Wound bed
Pelo epiKO
10dpw
b
Ctrl
Pelo epiKO
10dpw Itgα6 EdU DAPI
c
No. of epidermal EdU+ cells in wound bed (10dpw)
25
20
15
10
5
0
*
Ctrl
Pelo epiKO
d
Ctrl
Wound edge
Pelo epiKO
5dpw
e
No. of epidermal EdU+ cells in wound edge (5dpw)
80
70
60
50
40
30
20
10
0
*
Ctrl
Pelo epiKO
f
Ctrl
Wound edge
5dpw Itgα6 EdU DAPI
Pelo epiKO
g
Ctrl
Wound bed
Pelo epiKO
10dpw K14 K10 DAPI
h
Ctrl
Wound edge
5dpw K14 K10 DAPI
Pelo epiKO
i
Pelo fl/+; Lrig1 CreERT2; TdTom
+ 4OHT
Pelo fl/+; Lgr5 CreERT2; TdTom
+ 4OHT
Pelo fl/+; Lgr6 CreERT2; TdTom
+ 4OHT
TdTom DAPI
Pelo fl/fl; Lrig1 CreERT2; TdTom
+ 4OHT
Pelo fl/fl; Lgr5 CreERT2; TdTom
+ 4OHT
Pelo fl/fl; Lgr6 CreERT2; TdTom
+ 4OHT

Extended Data Figure 2. Delayed wound closure in *Pelo* null epidermis (a) Histology of skin 10 days post wound (dpw) shows delayed wound closure in *Pelo*^{epiKO}. (b, c) EdU staining of 10 dpw skin shows reduced proliferation in wound bed. Itgα6 staining demarcates dermal-epidermal boundary, Box indicates the wound bed (d) Histology of 5 dpw wound shows altered epidermal architecture. (e, f) EdU labelling of 5 dpw skin shows reduced proliferation at wound edge. (g, h) Immunostaining of Krt14 in 10 and 5 dpw skin shows abnormal differentiation in *Pelo*^{epiKO} (arrows). (i) TdTomato genetic labeling shows the contribution of Lrig1, Lgr5 and Lgr6 progeny in tail wound healing. Note that altered migration of Lrig1 cells in *Pelo*$^{fl/fl}$; *Lrig1*^{CreERT}; tdTom when compared to Lgr5 and Lgr6 on *Pelo* deletion. **p* = 0.0123 in (c), **p* = 0.0330 in (e). Scale bars, 100 μm.

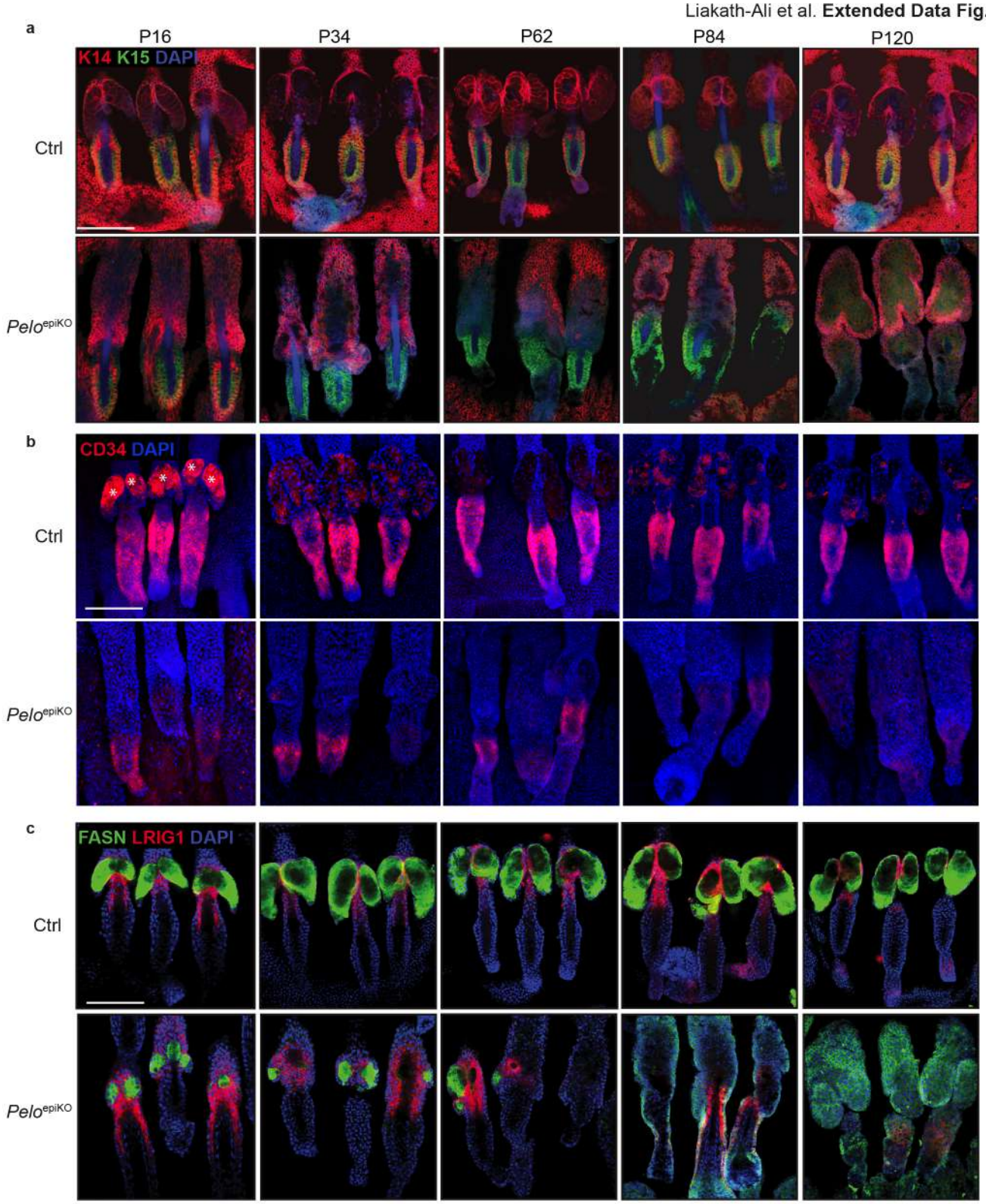
a
P16
P34
P62
P84
P120
K14 K15 DAPI
Ctrl
Pelo epiKO
b
CD34 DAPI
Ctrl
Pelo epiKO
c
FASN LRIG1 DAPI
Ctrl
Pelo epiKO

Extended Data Figure 3. *Pelo* deletion leads to progressive hair follicle and sebaceous gland abnormalities (a, b, c) Confocal images of tail epidermal wholemounts immunostained for Krt14, hair follicle bulge markers CD34 and Krt15, sebocyte maturation marker Fatty acid synthase (FASN) and junctional zone stem cell marker Lrig1 show progressive changes in hair follicle and sebaceous gland structure from P16 to P120 in $Pelo^{epiKO}$ mice. Note that the FASN staining in P84 and P120 $Pelo^{epiKO}$ epidermis is non-specific due to highly keratinized hair follicles. Asterisks in (b) indicate non-specific staining of sebaceous glands. Scale bars, 100 μm.

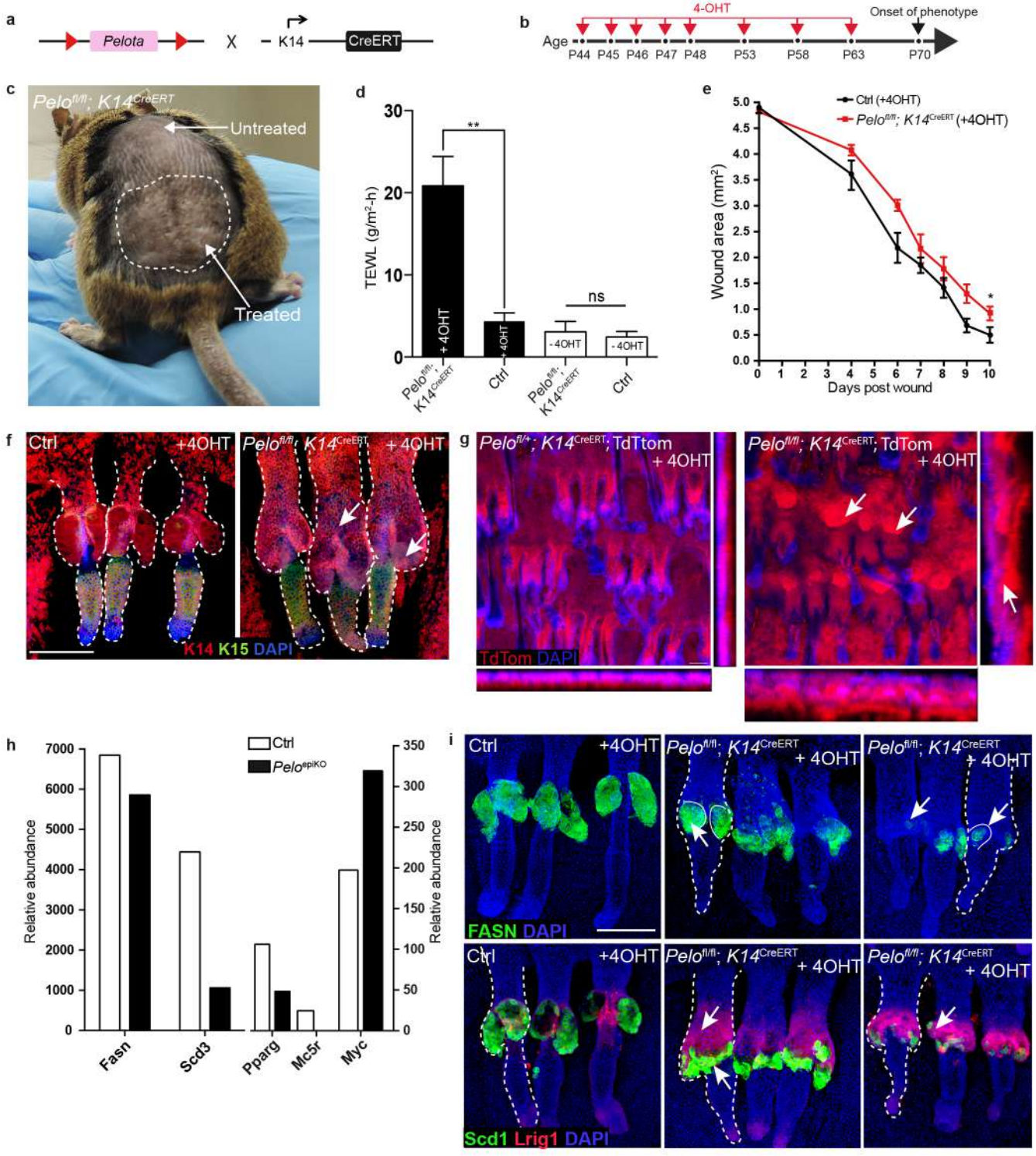
a
Pelota
X
K14
CreERT
b
4-OHT
Onset of phenotype
Age
P44 P45 P46 P47 P48 P53 P58 P63 P70
c
Pelofl/fl; K14CreERT
Untreated
Treated
d
TEWL (g/m2-h)
**
ns
+ 4OHT
- 4OHT
Pelofl/fl; K14CreERT
Ctrl
e
Ctrl (+4OHT)
Pelofl/fl; K14CreERT (+4OHT)
Wound area (mm2)
Days post wound
f
Ctrl +4OHT
Pelofl/fl; K14CreERT + 4OHT
K14 K15 DAPI
g
Pelofl/+; K14CreERT; TdTtom + 4OHT
Pelofl/fl; K14CreERT; TdTom + 4OHT
TdTom DAPI
h
Ctrl
PeloepiKO
Relative abundance
Fasn
Scd3
Pparg
Mc5r
Myc
i
Ctrl +4OHT
Pelofl/fl; K14CreERT + 4OHT
FASN DAPI
Scd1 Lrig1 DAPI

Extended Data Figure 4. Postnatal epidermal *Pelo* deletion impairs barrier function and wound healing (a, b) Breeding scheme and topical Tamoxifen (4-OHT) treatment regime. (c) Representative *Pelo*$^{fl/fl}$; *Krt14*^{CreERT} mouse showing skin lesions (dashed area) in 4-OHT-treated dorsal skin. (d) TEWL is increased in 4-OHT-treated skin of *Pelo*$^{fl/fl}$; *Krt14*^{CreERT}mice. (e) Rate of wound closure. (f) Tail epidermal wholemounts immunostained with Krt14 and Krt15 antibodies showing altered sebaceous gland architecture (arrows) in 4-OHT-treated *Pelo*$^{fl/fl}$; *Krt14*^{CreERT} mice. (g) Tail epidermal wholemounts from TdTomato (red) genetically labelled *Pelo*$^{fl/fl}$; *Krt14*^{CreERT} mice show keratinized cysts in hair follicles (arrows). (h) Cumulative mean values of gene expression obtained from ribosome profiling show down-regulation of markers of sebaceous gland differentiation and increase in Myc. (i) Tail epidermal wholemounts showing altered expression of FASN, Scd1 and Lrig1 (arrows) in sebaceous glands of 4-OHT-treated *Pelo*$^{fl/fl}$; *Krt14*^{CreERT} mice (middle and right panels). Dashed lines indicate pilosebaceous units. Scale bars, 100 μm. $^{**}p$ = 0.0072, $^{*}p$ = 0.0650, n. s., non significant. n = 3 in treated and untreated control groups.

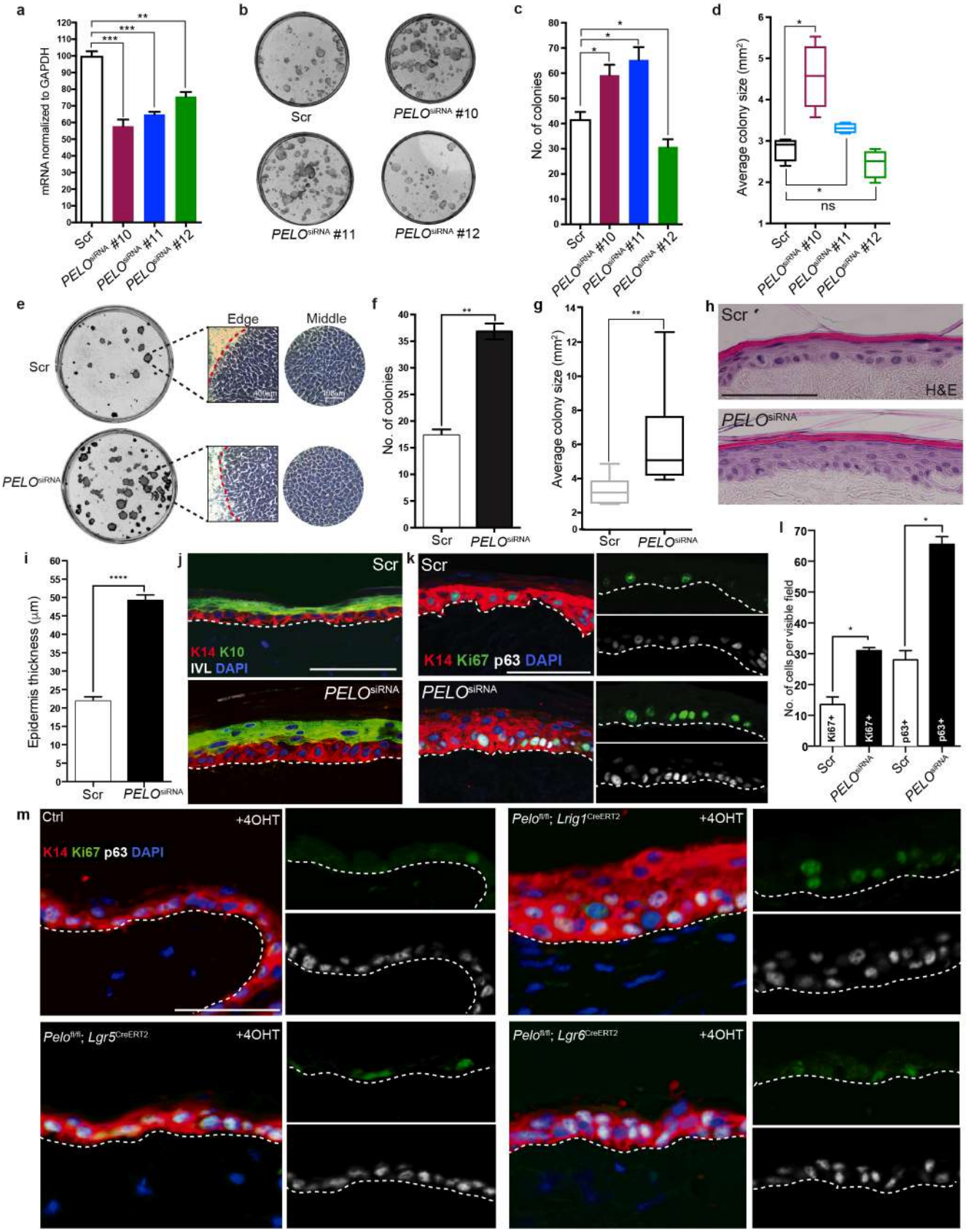
a
mRNA normalized to GAPDH
Scr
PELOsiRNA #10
PELOsiRNA #11
PELOsiRNA #12
b
Scr
PELOsiRNA #10
PELOsiRNA #11
PELOsiRNA #12
c
No. of colonies
d
Average colony size (mm²)
ns
e
Scr
Edge
Middle
PELOsiRNA
f
No. of colonies
g
Average colony size (mm²)
h
Scr
H&E
PELOsiRNA
i
Epidermis thickness (μm)
j
Scr
K14 K10
IVL DAPI
PELOsiRNA
k
Scr
K14 Ki67 p63 DAPI
PELOsiRNA
l
No. of cells per visible field
Ki67+
p63+
m
Ctrl
+4OHT
K14 Ki67 p63 DAPI
Pelofl/fl; Lrig1CreERT2
Pelofl/fl; Lgr5CreERT2
Pelofl/fl; Lgr6CreERT2

Extended Data Figure 5. Knockdown of *PELO* in human keratinocytes phenocopies mouse epidermal phenotype and proliferation difference in mice lacking Pelo in Lrig1, Lgr5 and Lgr6 stem cells. (a-d) PELO knockdown validation. (a) qRT-PCR for individual siRNAs transfected in human primary keratinocytes. (b) Clonal growth. (c, d) colony number and average size of individual colonies. (e-g) Clonal growth of keratinocytes, comparing pooled *PELO* siRNA knockdown ($PELO^{siRNA}$) and scrambled (Scr) control. (h-l) Effect of *PELO* knockdown in human epidermal reconstitution assay on decellularised dermis. (h, i) Epidermal thickness of DED cultures is significantly increased on *PELO* knockdown. (j-l) Immunolabelling for Krt14 (K14), Ki67, p63 and differentiation markers Krt10 (K10) and involucrin (IVL) shows increased number of differentiated cell layers (j) and increased number of cells expressing Ki67 and p63 (k, l) in $PELO^{siRNA}$ reconstituted epidermis. Dashed lines indicated dermal-epidermal boundary. Assessing proliferation by Ki67 and p63 in the dorsal skin IFE sections of mice lacking *Pelo* in Lrig1, Lgr5 and Lgr6 stem cells. Scale bars, 100 μm. ***p = 0.0009 (a, for siRNA#10), ***p = 0.0004 (a, for siRNA#11), **p = 0031 (a, for siRNA#12); *p = 0.0286 (c); *p = 0.0286 (d); **p = 0.0022 (f); **p = 0.0087 (g); ****p = < 0.0001 (i); *p = 0.0229 for Ki67 and *p = 0.0107 for p63 (l). n = 2 independent transfections; n = 3 dishes (a - g) and n = 2 sections of reconstituted epidermis (h, l).

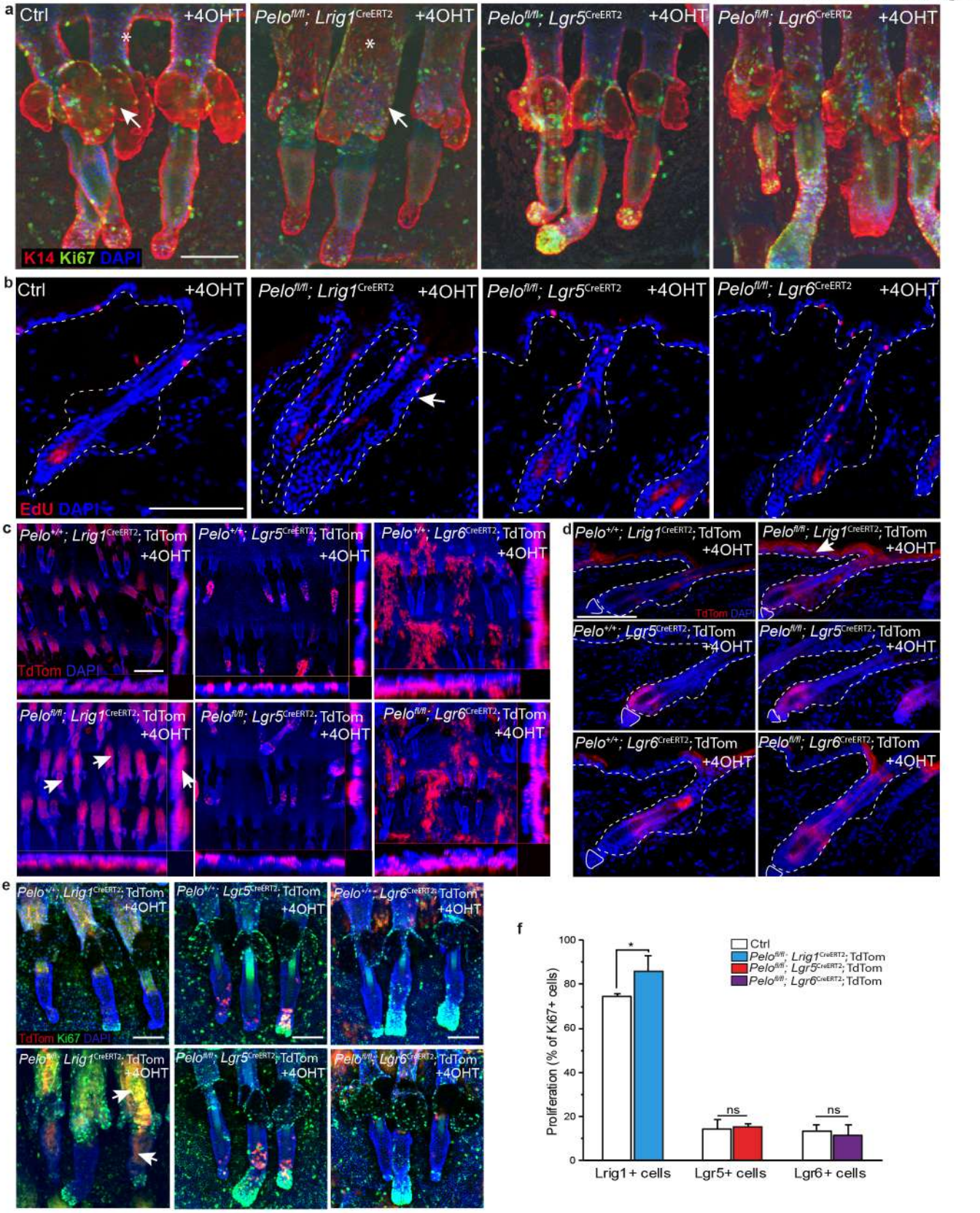
a
Ctrl +4OHT
Pelo fl/fl; Lrig1 CreERT2 +4OHT
Pelo fl/fl; Lgr5 CreERT2 +4OHT
Pelo fl/fl; Lgr6 CreERT2 +4OHT
K14 Ki67 DAPI
b
Ctrl +4OHT
Pelo fl/fl; Lrig1 CreERT2 +4OHT
Pelo fl/fl; Lgr5 CreERT2 +4OHT
Pelo fl/fl; Lgr6 CreERT2 +4OHT
EdU DAPI
c
Pelo +/+; Lrig1 CreERT2; TdTom +4OHT
Pelo +/+; Lgr5 CreERT2; TdTom +4OHT
Pelo +/+; Lgr6 CreERT2; TdTom +4OHT
Pelo fl/fl; Lrig1 CreERT2; TdTom +4OHT
Pelo fl/fl; Lgr5 CreERT2; TdTom +4OHT
Pelo fl/fl; Lgr6 CreERT2; TdTom +4OHT
TdTom DAPI
d
Pelo +/+; Lrig1 CreERT2; TdTom +4OHT
Pelo fl/fl; Lrig1 CreERT2; TdTom +4OHT
Pelo +/+; Lgr5 CreERT2; TdTom +4OHT
Pelo fl/fl; Lgr5 CreERT2; TdTom +4OHT
Pelo +/+; Lgr6 CreERT2; TdTom +4OHT
Pelo fl/fl; Lgr6 CreERT2; TdTom +4OHT
TdTom DAPI
e
Pelo +/+; Lrig1 CreERT2; TdTom +4OHT
Pelo +/+; Lgr5 CreERT2; TdTom +4OHT
Pelo +/+; Lgr6 CreERT2; TdTom +4OHT
Pelo fl/fl; Lrig1 CreERT2; TdTom +4OHT
Pelo fl/fl; Lgr5 CreERT2; TdTom +4OHT
Pelo fl/fl; Lgr6 CreERT2; TdTom +4OHT
TdTom Ki67 DAPI
f
Proliferation (% of Ki67+ cells)
100
80
60
40
20
0
*
ns
ns
Ctrl
Pelo fl/fl; Lrig1 CreERT2; TdTom
Pelo fl/fl; Lgr5 CreERT2; TdTom
Pelo fl/fl; Lgr6 CreERT2; TdTom
Lrig1+ cells
Lgr5+ cells
Lgr6+ cells

Extended Data Figure 6. Lrig1+ stem cells account for *Pelo* mutant epidermal phenotype (a) Tail epidermal wholemounts labeled with Krt14 and Ki67 antibodies, showing increased proliferation and alterations to the junctional zone (asterisks) and sebaceous glands (arrow) in *Pelo*$^{fl/fl}$; *Lrig1*^{CreERT2} mice. (b) Cross section of dorsal skin stained for EdU shows increased proliferation and alterations in HF infundibulum structure (arrow) in *Pelo*$^{fl/fl}$; *Lrig1*^{CreERT2} mice. (c-e) Confocal images of tail epidermal wholemounts (c, e) and dorsal skin sections (d) of tdTomato labelled *Pelo*$^{fl/fl}$; *Lrig1*^{CreERT2}, *Pelo*$^{fl/fl}$; *Lgr5*^{CreERT2} and *Pelo*$^{fl/fl}$; *Lgr6*^{CreERT2} mice. (c, d) Expansion of tdTomato-labelled Lrig1 (arrows) but not Lgr5 or Lgr6 progeny upon *Pelo* deletion. (e, f) Increase in proliferation (Ki67 labelling) of Lrig1 (arrows) but not Lgr5 and Lgr6 populations. Scale bars, 100 μm. *p = 0.0047 (f). n = 3-4 mice per group. All mice were in telogen of the hair cycle (2-3 months old) when treated with 4-OHT. Treatment regime and harvest of tissue were as indicated in Fig. 2c. Dashed lines mark epidermal-dermal boundary.

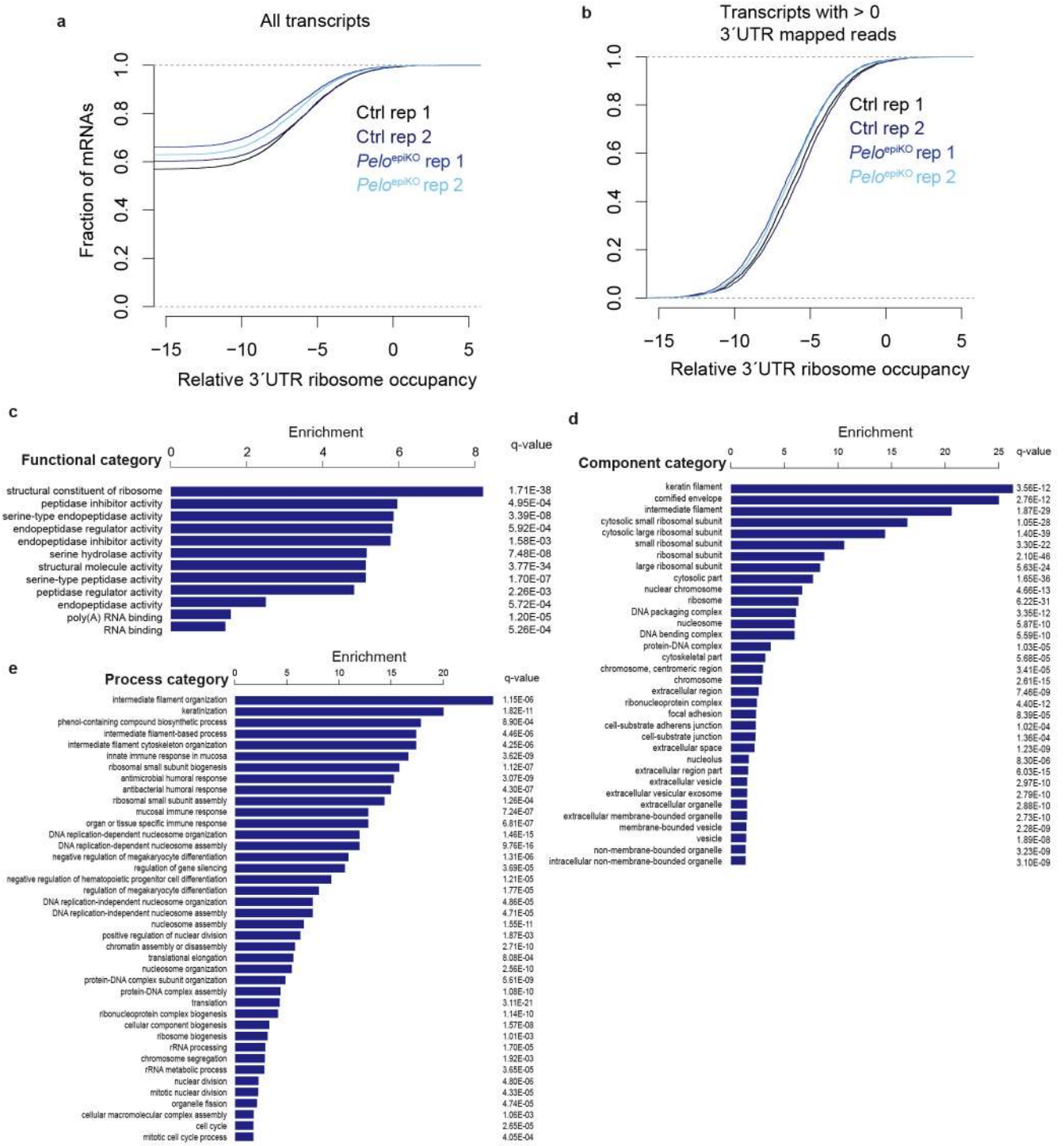
a
All transcripts
Fraction of mRNAs
0.0
0.2
0.4
0.6
0.8
1.0
Ctrl rep 1
Ctrl rep 2
Pelo epiKO rep 1
Pelo epiKO rep 2
−15
−10
−5
0
5
Relative 3´UTR ribosome occupancy
b
Transcripts with > 0
3´UTR mapped reads
Ctrl rep 1
Ctrl rep 2
Pelo epiKO rep 1
Pelo epiKO rep 2
Relative 3´UTR ribosome occupancy
c
Enrichment
Functional category
q-value
structural constituent of ribosome 1.71E-38
peptidase inhibitor activity 4.95E-04
serine-type endopeptidase activity 3.39E-08
endopeptidase regulator activity 5.92E-04
endopeptidase inhibitor activity 1.58E-03
serine hydrolase activity 7.48E-08
structural molecule activity 3.77E-34
serine-type peptidase activity 1.70E-07
peptidase regulator activity 2.26E-03
endopeptidase activity 5.72E-04
poly(A) RNA binding 1.20E-05
RNA binding 5.26E-04
d
Enrichment
Component category
q-value
keratin filament 3.56E-12
cornified envelope 2.76E-12
intermediate filament 1.87E-29
cytosolic small ribosomal subunit 1.05E-28
cytosolic large ribosomal subunit 1.40E-39
small ribosomal subunit 3.30E-22
ribosomal subunit 2.10E-46
large ribosomal subunit 5.63E-24
cytosolic part 1.65E-36
nuclear chromosome 4.66E-13
ribosome 6.22E-31
DNA packaging complex 3.35E-12
nucleosome 5.87E-10
DNA bending complex 5.59E-10
protein-DNA complex 1.03E-05
cytoskeletal part 5.68E-05
chromosome, centromeric region 3.41E-05
chromosome 2.61E-15
extracellular region 7.46E-09
ribonucleoprotein complex 4.40E-12
focal adhesion 8.39E-05
cell-substrate adherens junction 1.02E-04
cell-substrate junction 1.36E-04
extracellular space 1.23E-09
nucleolus 8.30E-06
extracellular region part 6.03E-15
extracellular vesicle 2.97E-10
extracellular vesicular exosome 2.79E-10
extracellular organelle 2.88E-10
extracellular membrane-bounded organelle 2.73E-10
membrane-bounded vesicle 2.28E-09
vesicle 1.89E-08
non-membrane-bounded organelle 3.23E-09
intracellular non-membrane-bounded organelle 3.10E-09
e
Enrichment
Process category
q-value
intermediate filament organization 1.15E-06
keratinization 1.82E-11
phenol-containing compound biosynthetic process 8.90E-04
intermediate filament-based process 4.46E-06
intermediate filament cytoskeleton organization 4.25E-06
innate immune response in mucosa 3.62E-09
ribosomal small subunit biogenesis 1.12E-07
antimicrobial humoral response 3.07E-09
antibacterial humoral response 4.30E-07
ribosomal small subunit assembly 1.26E-04
mucosal immune response 7.24E-07
organ or tissue specific immune response 6.81E-07
DNA replication-dependent nucleosome organization 1.46E-15
DNA replication-dependent nucleosome assembly 9.76E-16
negative regulation of megakaryocyte differentiation 1.31E-06
regulation of gene silencing 3.69E-05
negative regulation of hematopoietic progenitor cell differentiation 1.21E-05
regulation of megakaryocyte differentiation 1.77E-05
DNA replication-independent nucleosome organization 4.86E-05
DNA replication-independent nucleosome assembly 4.71E-05
nucleosome assembly 1.55E-11
positive regulation of nuclear division 1.87E-03
chromatin assembly or disassembly 2.71E-10
translational elongation 8.08E-04
nucleosome organization 2.56E-10
protein-DNA complex subunit organization 5.61E-09
protein-DNA complex assembly 1.08E-10
translation 3.11E-21
ribonucleoprotein complex biogenesis 1.14E-10
cellular component biogenesis 1.57E-08
ribosome biogenesis 1.01E-03
rRNA processing 1.70E-05
chromosome segregation 1.92E-03
rRNA metabolic process 3.65E-05
nuclear division 4.80E-06
mitotic nuclear division 4.33E-05
organelle fission 4.74E-05
cellular macromolecular complex assembly 1.06E-03
cell cycle 2.65E-05
mitotic cell cycle process 4.05E-04

Extended Data Figure 7. *Pelo* knockout epidermal cells do not accumulate 3′UTR footprints (a) Empiric cumulative distribution plots of relative 3′UTR ribosome occupancy for all transcripts or (b) those with at least 1 read mapped to the 3′UTR. (c-e) Gene Ontology of genes differentially expressed in *Pelo*-null epidermis. Functional, component and process categories of genes enriched in $Pelo^{epiKO}$.

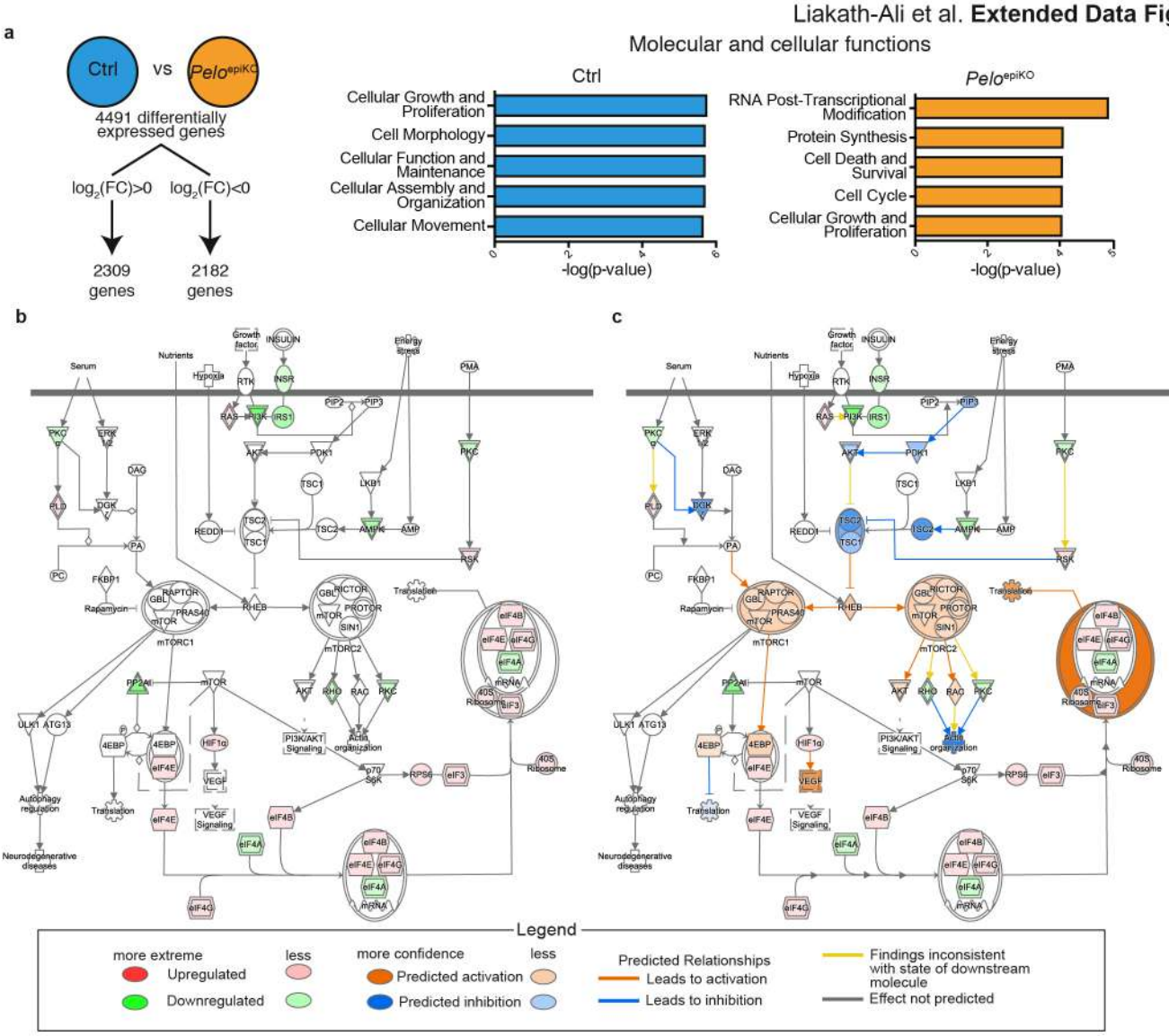
a
Ctrl
vs
Pelo epiKO
4491 differentially expressed genes
log2(FC)>0
log2(FC)<0
2309 genes
2182 genes
Molecular and cellular functions
Ctrl
Cellular Growth and Proliferation
Cell Morphology
Cellular Function and Maintenance
Cellular Assembly and Organization
Cellular Movement
-log(p-value)
Pelo epiKO
RNA Post-Transcriptional Modification
Protein Synthesis
Cell Death and Survival
Cell Cycle
Cellular Growth and Proliferation
-log(p-value)
b
c
Legend
more extreme
Upregulated
Downregulated
less
more confidence
Predicted activation
Predicted inhibition
less
Predicted Relationships
Leads to activation
Leads to inhibition
Findings inconsistent with state of downstream molecule
Effect not predicted

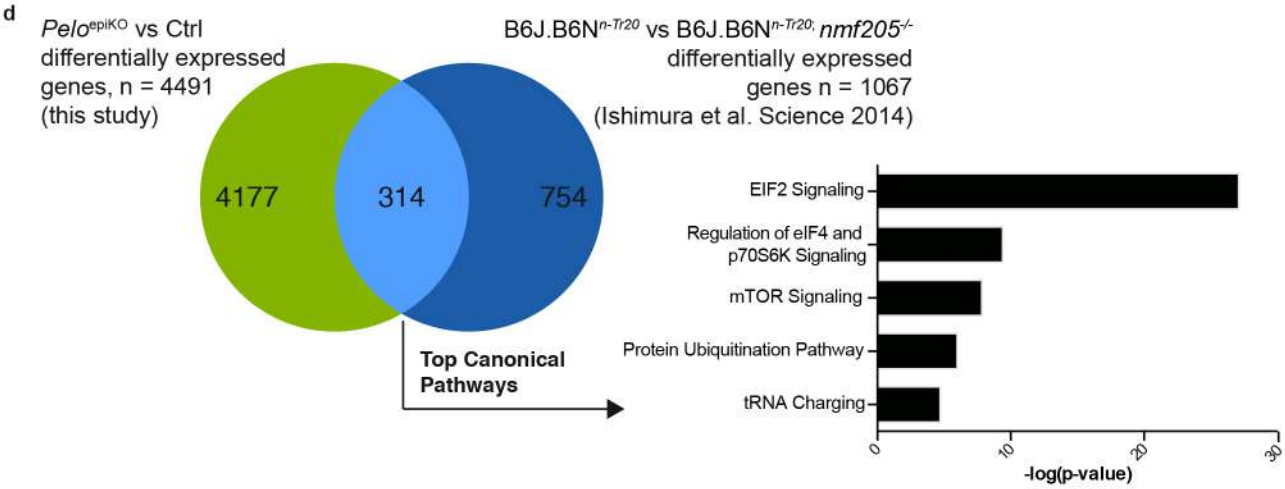
d
Pelo epiKO vs Ctrl differentially expressed genes, n = 4491 (this study)
B6J.B6N n-Tr20 vs B6J.B6N n-Tr20; nmf205 -/- differentially expressed genes n = 1067 (Ishimura et al. Science 2014)
4177
314
754
Top Canonical Pathways
EIF2 Signaling
Regulation of eIF4 and p70S6K Signaling
mTOR Signaling
Protein Ubiquitination Pathway
tRNA Charging
-log(p-value)

Extended Data Figure 8. Computational analysis of differentially regulated pathways between control and *Pelo*^{epiKO} and comparison of molecular signatures in *Pelo*^{epiKO} and Gtpbp2-deficient brain (a) Number of genes that were differentially expressed in *Pelo*^{epiKO} and control epidermis and their associated functions. (b, c) Ingenuity Pathway Analysis showing changes in mTOR pathway genes in *Pelo*^{epiKO} vs control epidermis (b) and their predicted molecular activities (c). (d) Venn diagram shows common differentially expressed genes in our study and that of Ishimura et al (2014) when comparing Ctrl and mutants. The 314 overlapping genes are enriched in top canonical pathways that are highly related to translation.

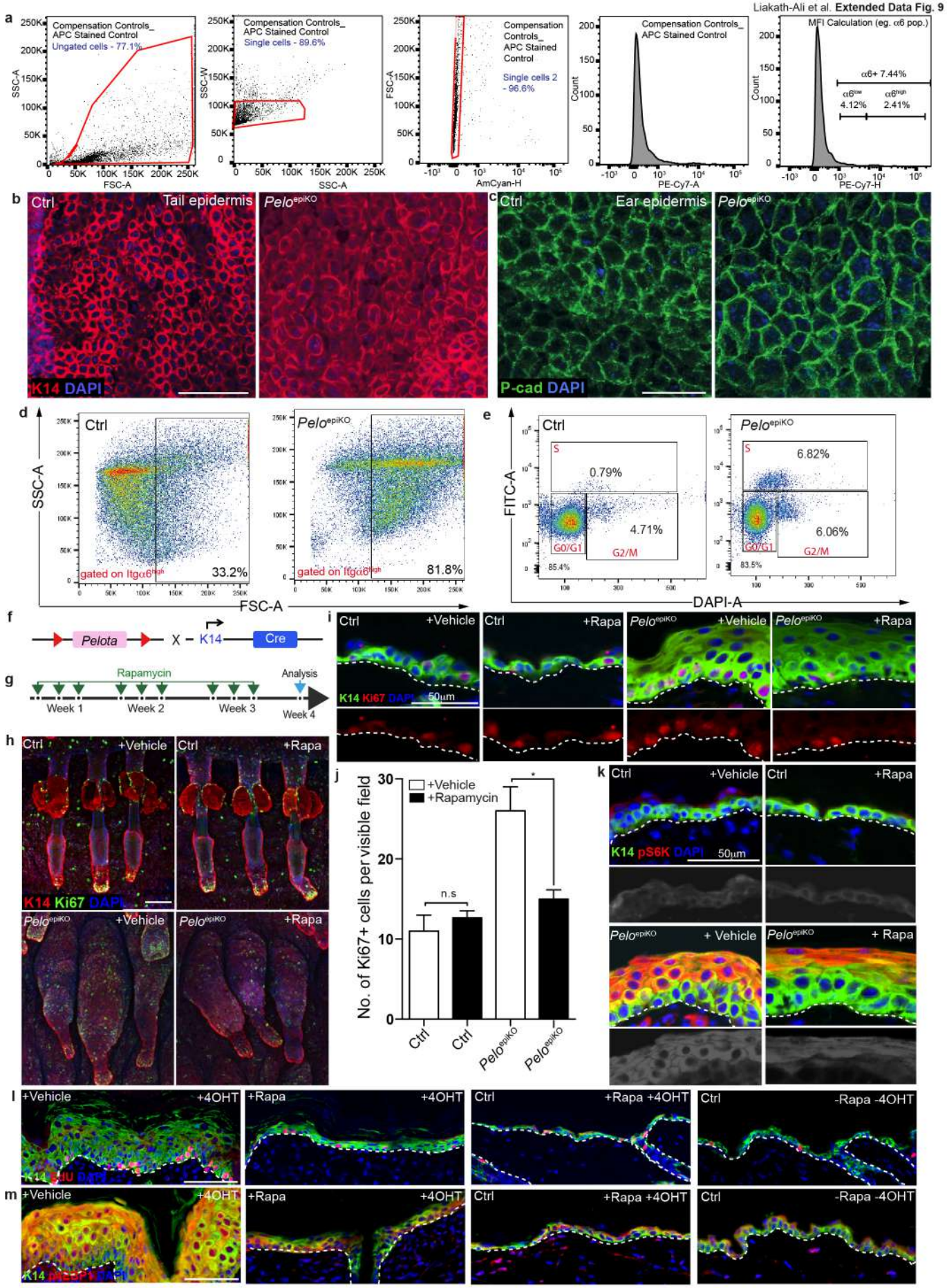
a
Compensation Controls_ APC Stained Control
Ungated cells - 77.1%
Single cells - 89.6%
Single cells 2 - 96.6%
MFI Calculation (eg. α6 pop.)
α6+ 7.44%
α6low 4.12%
α6high 2.41%
b
Ctrl
Tail epidermis
Pelo epiKO
K14 DAPI
c
Ctrl
Ear epidermis
Pelo epiKO
P-cad DAPI
d
Ctrl
Pelo epiKO
gated on Itgα6high
33.2%
81.8%
e
S
0.79%
4.71%
G0/G1
G2/M
85.4%
6.82%
6.06%
83.5%
f
Pelota
X
K14
Cre
g
Rapamycin
Analysis
Week 1
Week 2
Week 3
Week 4
i
Ctrl +Vehicle
Ctrl +Rapa
Pelo epiKO +Vehicle
Pelo epiKO +Rapa
K14 Ki67 DAPI
50μm
h
K14 Ki67 DAPI
j
+Vehicle
+Rapamycin
No. of Ki67+ cells per visible field
n.s
*
Ctrl
Pelo epiKO
k
K14 pS6K DAPI
50μm
+ Vehicle
+ Rapa
l
+Vehicle
+4OHT
+Rapa
Ctrl
+Rapa +4OHT
-Rapa -4OHT
m
K14 pS6RP DAPI

Extended Data Figure 9. *Pelo* epidermal deletion results in increased protein synthesis and basal stem cell size and Rapamycin treatment reduces proliferation of *Pelo*-null epidermis

(a) Gating strategy for measurement of OP-Puromycin incorporation in cell populations (b, c) Confocal images of tail and ear epidermal wholemounts immunolabelled for Krt14 and P-cadherin (P-Cad), showing IFE basal cells. (d, e) Representative flow cytometric dot plot showing increased cell size (FSC-A) of Itgα6^{high} cells and altered S and G2/M cell cycle phases in *Pelo*^{epiKO} epidermis. (f, g) Breeding scheme and rapamycin treatment regime. (h) Immunolabelling of tail epidermal wholemounts with Krt14 and Ki67 antibodies shows reduced proliferation in rapamycin-treated mice compared to vehicle-treated group. Note that there was no significant change in epidermal proliferation of control mice treated with rapamycin when compared to vehicle treated mice. (i, j) Cross sections of IFE from *Pelo*^{epiKO} and control back skin immunolabelled with Krt14 and Ki67 antibodies, showing significant reduction in Ki67+ and suprabasal Krt14+ cells in rapamycin-treated compared to vehicle-treated mice. (k) Cross sections of IFE from control and *Pelo*^{epiKO} back skin immunolabelled with Krt14 and pS6K antibodies showing marked increase in pS6K labeling indicating mTOR hyperactivation in vehicle-treated *Pelo*^{epiKO} skin. (l) Cross sections of IFE of control and *Pelo*$^{fl/fl}$; *Krt14*^{CreERT} mice (with simultaneous 4-OHT and Rapamycin treatment) immunolabelled for Krt14 and EdU showing significant reduction in EdU+ and suprabasal Krt14+ cells in rapamycin-treated compared to vehicle-treated mice. (m) Cross sections of IFE of control and *Pelo*$^{fl/fl}$; *Krt14*^{CreERT} mice (with simultaneous 4-OHT and Rapamycin treatment) immunolabelled for Krt14 and p4EBP antibodies. Note reduced pS6K labeling (k) and p4EBP1 (m) in rapamycin-treated epidermis. Gray scale images for pS6K are

shown below merged images. Scale bars, 100 μm. *p = 0.0132 in (j), n. s., non significant. n = 3 mice in all groups. Dashed lines mark epidermal-dermal boundary.

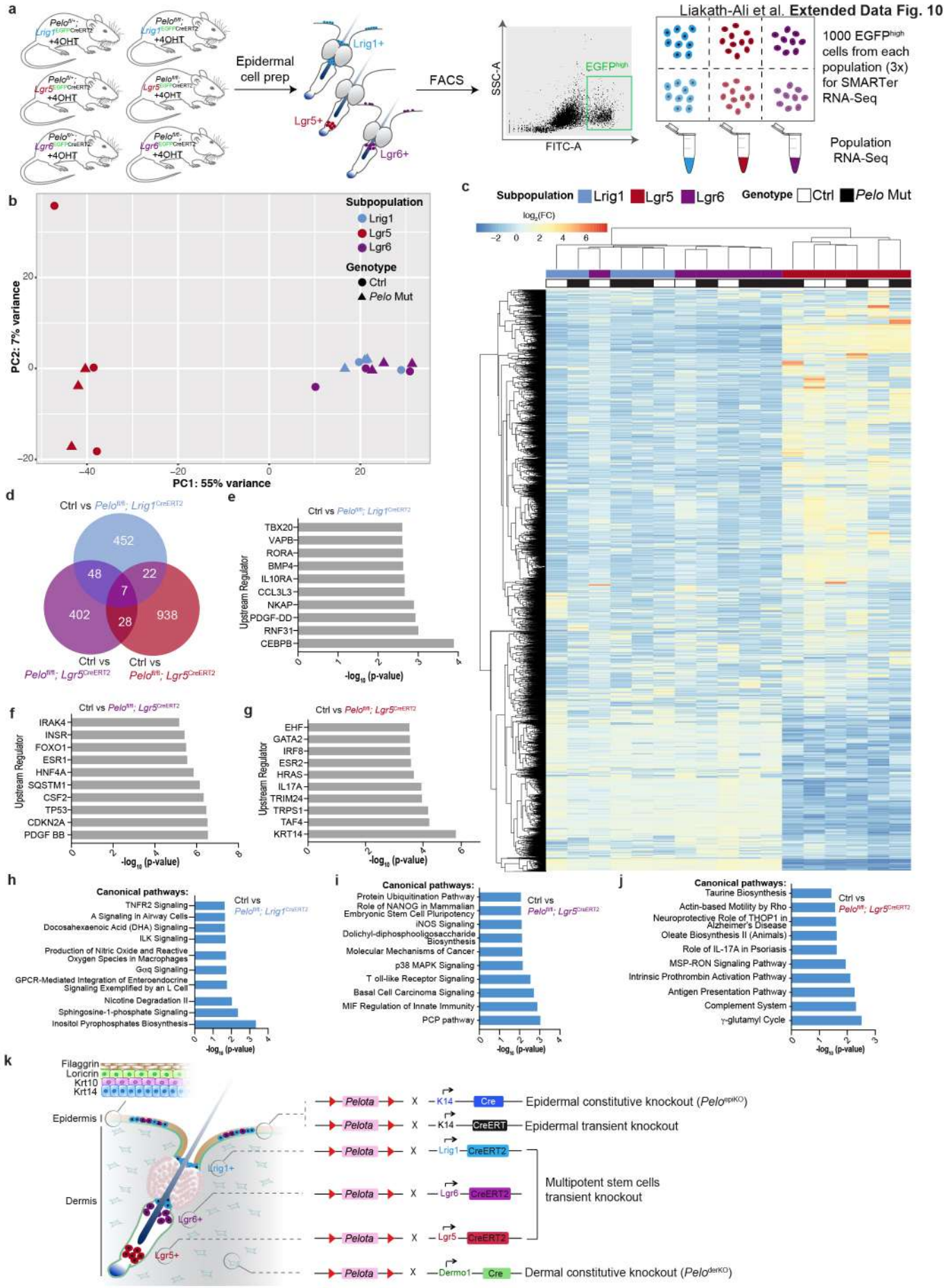
Liakath-Ali et al. Extended Data Fig. 10
a
+4OHT
Epidermal cell prep
Lrig1+
Lgr5+
Lgr6+
FACS
SSC-A
FITC-A
EGFPhigh
1000 EGFPhigh cells from each population (3x) for SMARTer RNA-Seq
Population RNA-Seq
b
Subpopulation
Lrig1
Lgr5
Lgr6
Genotype
Ctrl
Pelo Mut
PC2: 7% variance
PC1: 55% variance
c
Subpopulation Lrig1 Lgr5 Lgr6
Genotype Ctrl Pelo Mut
log2(FC)
d
Ctrl vs Pelofl/fl; Lrig1CreERT2
452
48
22
7
402
28
938
Ctrl vs Pelofl/fl; Lgr5CreERT2
Ctrl vs Pelofl/fl; Lgr6CreERT2
e
Ctrl vs Pelofl/fl; Lrig1CreERT2
Upstream Regulator
TBX20
VAPB
RORA
BMP4
IL10RA
CCL3L3
NKAP
PDGF-DD
RNF31
CEBPB
-log10 (p-value)
f
Ctrl vs Pelofl/fl; Lgr5CreERT2
Upstream Regulator
IRAK4
INSR
FOXO1
ESR1
HNF4A
SQSTM1
CSF2
TP53
CDKN2A
PDGF BB
-log10 (p-value)
g
Ctrl vs Pelofl/fl; Lgr5CreERT2
Upstream Regulator
EHF
GATA2
IRF8
ESR2
HRAS
IL17A
TRIM24
TRPS1
TAF4
KRT14
-log10 (p-value)
h
Canonical pathways:
Ctrl vs Pelofl/fl; Lrig1CreERT2
TNFR2 Signaling
A Signaling in Airway Cells
Docosahexaenoic Acid (DHA) Signaling
ILK Signaling
Production of Nitric Oxide and Reactive Oxygen Species in Macrophages
Gαq Signaling
GPCR-Mediated Integration of Enteroendocrine Signaling Exemplified by an L Cell
Nicotine Degradation II
Sphingosine-1-phosphate Signaling
Inositol Pyrophosphates Biosynthesis
-log10 (p-value)
i
Canonical pathways:
Ctrl vs Pelofl/fl; Lgr5CreERT2
Protein Ubiquitination Pathway
Role of NANOG in Mammalian Embryonic Stem Cell Pluripotency
iNOS Signaling
Dolichyl-diphosphooligosaccharide Biosynthesis
Molecular Mechanisms of Cancer
p38 MAPK Signaling
T cell-like Receptor Signaling
Basal Cell Carcinoma Signaling
MIF Regulation of Innate Immunity
PCP pathway
-log10 (p-value)
j
Canonical pathways:
Ctrl vs Pelofl/fl; Lgr5CreERT2
Taurine Biosynthesis
Actin-based Motility by Rho
Neuroprotective Role of THOP1 in Alzheimer's Disease
Oleate Biosynthesis II (Animals)
Role of IL-17A in Psoriasis
MSP-RON Signaling Pathway
Intrinsic Prothrombin Activation Pathway
Antigen Presentation Pathway
Complement System
γ-glutamyl Cycle
-log10 (p-value)
k
Filaggrin
Loricrin
Krt10
Krt14
Epidermis
Dermis
Lrig1+
Lgr6+
Lgr5+
Pelota X K14 Cre Epidermal constitutive knockout (PeloepiKO)
Pelota X K14 CreERT Epidermal transient knockout
Pelota X Lrig1 CreERT2
Pelota X Lgr6 CreERT2
Pelota X Lgr5 CreERT2
Multipotent stem cells transient knockout
Pelota X Dermo1 Cre Dermal constitutive knockout (PeloderKO)

Extended Data Figure 10. RNA-sequencing of Lrig1+, Lgr5+ and Lgr6+ cells reveals Lgr5 as a transcriptionally unique subpopulation and subtle changes in transcription in all subpopulations when *Pelo* is deleted. (a) Schematic illustration of the EGFP^{high} sorting and RNA-seq strategy for control and *Pelo*-deleted subpopulations using *Pelo*$^{fl/fl}$; *Lrig1*$^{EGFP\text{-}CreERT2}$, *Pelo*$^{fl/fl}$; L*gr5*$^{EGFP\text{-}CreERT2}$ and *Pelo*$^{fl/fl}$; *Lgr6*$^{EGFP\text{-}CreERT2}$ mice. (b) Principal component analysis of RNA-seq data shows that the Lgr5 subpopulation is remarkably different from the other two. Note that there is no major change in the clusters when *Pelo* is deleted in any of the subpopulations. (c) Hierarchical clustering of the subpopulations corroborates minimal transcriptional changes between control and Mut mice, revealing two major clusters, one for Lgr5 and another for Lrig1 and Lgr6. (d) Venn diagram illustrating the differentially expressed genes in common between the 3 subpopulations when comparing control and Mut. (e) Top differentially regulated transcription factors between Lrig1 and Lgr5 (f), Lgr5 and Lgr6 (g) and Lrig1 and Lgr6 control subpopulations. (h-j) Top differentially regulated canonical pathways between Lrig1 and Lgr5 (h), Lgr5 and Lgr6 (i) and Lrig1 and Lgr6 control subpopulations (j). (k) Schematic of epidermis showing location of marker expression and the various transgenic mice used in this study.